Research Square

Preprints are preliminary reports that have not undergone peer review.
They should not be considered conclusive, used to inform clinical practice,
or referenced by the media as validated information.

Ocean Temperature-Regulated Dichotomy of Carbon Isotopes in Post-Marinoan Badami Carbonates, India

Rachita Ghosh
Indian Institute of Science Bangalore
Prosenjit Ghosh
pghosh@iisc.ac.in
Indian Institute of Science Bangalore
Arunava Sen
Jadavpur University, Kolkata
Soumik Mukhopadhyay
Jadavpur University, Kolkata
Pradip Samanta
University of North Bengal, Darjeeling, Siliguri

Research Article

Keywords: Ediacaran, Clumped isotope thermometry, Badami, Organic matter decomposition, Depositional environment

Posted Date: April 10th, 2026

DOI: https://doi.org/10.21203/rs.3.rs-9363750/v1

License: This work is licensed under a Creative Commons Attribution 4.0 International License. Read Full License

Additional Declarations: The authors declare no competing interests.

Abstract

The post-Marinoan Snowball Earth witnessed rapid carbonate deposition on marine platforms worldwide. Evidence of organic matter degradation, alkalinity development and carbonate precipitation is present in the sedimentary record. A diverging trend in the carbon isotopic value of inorganic and organic carbon is proposed here as a proxy for organic alkalinity. The carbon isotopic signatures in the organic matter and carbonate precipitates, along with temperature estimates, indicate that organic matter degradation is regulated by rising temperatures. The clumped-isotopic composition of post-Marinoan Badami carbonates strongly suggests that low-Mg carbonates are pristine, providing a unique window into the carbon cycle processes. These carbonates record a lower temperature end-member in the range of 2 to 26°C with abundant presence of total organic carbon (TOC). In contrast, samples with higher temperatures are dolomitic and contain low TOC. The partitioning of carbon isotopes between organic and inorganic phases enables tracing the source of dissolved carbon species derived from organic matter degradation in the shallow, equatorial, oxygenated marine environment, and is modelled using the Rayleigh fractionation approach. The magnitude of the isotopic signature present in the Badami carbonates exhibits a clear depositional control, similar to the neighbouring Neoproterozoic Doushantuo Formation in South China.

Highlights

- Badami carbonate records the primary Ediacaran tropical seawater temperature.
- The decomposition of organic matter, regulated by ambient temperature, generates alkalinity and promotes carbonate precipitation.
- Latitudinal variation of $\delta^{13}C_{Carb}$ of post-Marinoan carbonates reflects relative AOU variation in Ediacaran oceans.
- Depositional environment controls $\delta^{13}C_{Carb}$, $\delta^{13}C_{Org}$ trends and organic-matter preservation.

1. Introduction

The Neoproterozoic postglacial ocean provides a time window marking the dawn of complex macroscopic life evolution, when the Marinoan Snowball Earth deglaciated in response to atmospheric CO_2 buildup and the planet subsequently warmed (Ramme et al., 2024). The ecological and sedimentary framework for the organic evolution and development of soft-bodied creatures, popularly known as the Ediacaran fauna, was developed under conditions of efficient environmental CO_2 sequestration, reflected in enhanced organic carbon burial and extensive carbonate precipitation. The Ediacaran period is marked by a global record of carbonate deposition in shallow marine environments, predominantly along the paleotropical shoreline (Li et al., 2013). These carbonate deposits were underlain by an organic-rich, muddy substratum that served as an efficient alkaline buffer, retaining remineralised carbon, produced by the decomposition of organic matter, within the dissolved inorganic carbon pool and promoting carbonate precipitation. Alkalinity development was facilitated by multiple degradation pathways, including ammonification of organic nitrogen and decarboxylation of organic acids during organic matter decomposition, leading to pH elevation (Rukshana, 2012; Van Ryckel et al., 2025). The efficiency of organic matter degradation and associated alkalinity production was further regulated by the thermal state and oxygen availability in the sediment-water column, particularly in semi-enclosed basin settings (Chen et al., 2022). In the absence of terrestrial vegetation, reduced smectite formation in continental catchments favoured illite-dominated clay assemblages on carbonate platforms (Hazen et al., 2013; Tosca et al., 2010), which may have further enhanced the buffering capacity of shelf sediments by increasing alkali metal retention.

The Neoproterozoic post-glacial carbonate deposits are commonly dolomitic (Thomas and Catling, 2024; Yu et al., 2020), formed through the interplay of processes such as burial, early diagenesis, and hydrothermal activity (Sepeda et al., 2024). Rarely, these deposits experience limited burial diagenesis, as they were originally calcitic and later transformed to dolomitic or high-Mg calcite, a factor that has been described as responsible for the reordering of the clumped-isotopic composition (Bergmann et al., 2025; Chang et al., 2020). The presence of well-preserved sedimentary carbonates that retain pristine depositional conditions makes the Badami sedimentary archive unique (George et al., 2023) for assessing the roles of temperature and water chemistry in organic carbon burial and CO_2 uptake through productivity and carbonate deposition. Sedimentary carbonate records integrate the net effects of carbon cycling, reflecting the interplay between photosynthesis and organic degradation through sedimentary processes such as deposition, compaction, and burial diagenesis. The Neoproterozoic marine sedimentary environment, characterised by the presence of organic matter (OM), exhibits evidence of biological productivity that is likely regulated by the nutrient supply through continental runoff, coastal upwelling and hydrothermal fluid effused from shallow rift zones (Bristow et al., 2009; Laakso and Schrag, 2019; Ye et al., 2025).

In this study, the stable isotope geochemistry ($\delta^{13}C_{Carb}$, $\delta^{13}C_{Org}$, and TOC) of the Neoproterozoic Badami carbonates from southern India is compared with that of a time-equivalent section from the Doushantuo Formation in South China, both representing a low-latitude marine environment. The multiple lithological sections of the Doushantuo Formation, with well-characterised sedimentological features, provide a basis for reconstructing depositional environments (Jiang et al., 2011), which were further correlated with the depositional setting inferred for the Badami carbonates. Moreover, Chemostratigraphic correlation of the carbon isotope profiles with the Doushantuo Formation constrains the depositional age of the Badami carbonates to ~626-591 Ma. This uninterrupted sedimentation during this time interval provides a reliable framework for investigating the evolution of the post-Marinoan tropical marine environment. The carbon isotopic composition of the Badami carbonate ($\delta^{13}C_{Carb}$), when integrated with global records, provides insight into the spatial pattern of the global oceanic carbon cycle following the Marinoan deglaciation. We used carbonate clumped-isotope-based temperature estimates, $\delta^{13}C$ of OM, and TOC content from Badami carbonates to model the thermally modulated biodegradation process in a shallow marine, oxygenated depositional setting and demonstrated its efficiency in carbonate precipitation.

2. Materials and Methods

Nineteen rock samples were collected from a ~20 m thick outcrop section exposed near Konkankoppa village (16°1'13.98"N, 75°38'57.46"E) and divided into two portions: one for bulk powdering and the other for preparing polished slabs for retrieving drilled powders from specific spots. Bulk powders were produced using an agate mortar, while spot powders were obtained with a hand-held microdrill (0.5-1 mm stainless steel bits). In total, 38 powdered samples (19 bulk and 19 point-drilled) were prepared for isotopic analyses of inorganic carbonates, and the 19 bulk powders were also used for XRD analysis and the geochemical study of organic matter.

2.1. Measurement of total organic carbon content (TOC) and carbon isotopic composition of bulk organic matter ($\delta^{13}C_{Org}$)

About 20 mg of each bulk powder was reacted with 1N HCl at room temperature for three days to remove any inorganic carbonates. The acid was replaced multiple times until effervescence ceased, followed by repeated washing with Milli-Q water until a neutral pH was achieved. Furthermore, the treated powders were dried overnight at 60°C. Approximately 10 mg of the decarbonated residue was then loaded inside tin capsules for TOC and $\delta^{13}C_{Org}$ measurement. Samples were combusted at 850°C inside a quartz reactor equipped with a Cr_2O_3 catalyst using a FLASH 2000 Elemental Analyser (Thermo Scientific), converting organic carbon to CO_2, which was analysed using a Finnigan Delta V IRMS (Thermo Scientific) interfaced via a CONFLO-IV interface. The $\delta^{13}C_{Org}$ values were corrected using internal standards Oasis_glucose ($\delta^{13}C_{VPDB}$= −10.99‰) and Oasis_Rice_1 ($\delta^{13}C_{VPDB}$= −27.67‰), calibrated against IAEA-CH6 sucrose ($\delta^{13}C_{VPDB}$= −10.45‰), yielding an analytical reproducibility of ±0.12‰ (1σ, n=10) (Kaushal and Ghosh, 2018).

Mass of carbon in the sample was determined using the linear relationship between total CO_2 peak area (sum of the mass 44, 45 and 46 peak areas obtained from IRMS measurements) and carbon content, constructed by measuring pure Oasis_glucose (contains 40% C), with amounts ranging from 0.04 to 0.1 mg. The TOC content was then calculated using the following equation:

TOC (wt%) = (mass of carbon in the sample/ total mass of the sample) * 100%.

2.2. Inorganic Carbon, Oxygen Isotope and Carbonate clumped Isotope analysis

About 10–15mg of finely powdered sample was reacted with 2ml of orthophosphoric acid (density 1.94 g/cm³) in a sealed Pyrex reaction vessel under 10^{-3} mbar pressure at room temperature (Fosu et al., 2019). The vessels were then kept in a 25°C water bath for 24 hours for calcitic and 72 hours for dolomitic carbonates. The reaction liberates CO_2 from carbonate powder during acid digestion,

$CaCO_3(s) + H_3PO_4(l) = CaHPO_4(s) + CO_2(g) + H_2O(g)$

CO_2 was cryogenically extracted from the reaction vessel using liquid N_2 (−196°C) following the procedure described in the break-seal method (Fosu et al., 2019), then purified of polar compounds, which act as contaminants (e.g., haloalkanes, H_2O) via a Porapak-Q gas chromatograph (2m length, 1/8” diameter, 80/100 mesh) maintained at 25°C. The GC column was heated to 150°C for 2 hours after each sample purification to remove accumulated contaminants. Isotopic masses of CO_2 (44 to 49) were measured relative to the laboratory working gas (Linde CO_2) using a dual inlet peripheral connected with Finnigan MAT 253 IRMS (Thermo Scientific). Each sample CO_2 gas was measured against the working gas for 10 cycles, designated as one acquisition. Ten acquisitions define a batch for single-sample measurement. Therefore, each measurement consists of 100 cycles of alternating sample and reference injections. Linde CO_2 was calibrated against NBS-19, assigned $\delta^{13}C_{VPDB}$= −3.92‰ and $\delta^{18}O_{VSMOW}$= 25.58‰. Residual CO_2, when sufficient, was retrieved, sealed in quartz tubes, and heated at 1000°C for 3 h in a muffle furnace to produce heated gas (HG) (Ghosh et al., 2006), which was measured after every three samples. Two internal reference carbonates (MARJ1 & OMC) and four international (ETH1, ETH2, ETH3 & ETH4) carbonates were analysed following the same protocol. During most analyses, the primary ion beam intensity was maintained between 10,000 and 12,000 mV.

$\delta^{13}C_{Carb}$ and $\delta^{18}O_{Carb}$ were derived from the intensity of CO_2 mass 45 and 46, respectively. Laboratory reference material MARJ1($\delta^{13}C_{VPDB}$ = 1.97‰ & $\delta^{18}O_{VPDB}$ = -2.02‰), independently calibrated with NBS-19, was used to evaluate $\delta^{13}C_{Carb}$ and $\delta^{18}O_{Carb}$ of samples. The stable and clumped isotopic composition (Δ_{47}) of all samples is given in Table 1. Δ_{47} values were obtained from CO_2 mass-47 intensities and converted to the heated gas scale ($\Delta_{47(HGS)}$) using a weighted regression of HGs with varying bulk isotopic compositions (δ^{47} values). These were further converted to the absolute reference frame (ARF scale, $\Delta_{47(ARF)}$) (Dennis et al., 2011), using MARJ1, OMC, ETH1, and ETH3, with accepted $\Delta_{47(ARF)}$ values of 0.395 ± 0.002‰, 0.587 ± 0.004‰, 0.271 ± 0.005‰, and 0.698 ± 0.005‰, respectively (Fosu et al., 2019). Sample $\Delta_{47(ARF)}$ values range from 0.35‰ to 0.81‰ (n=47) with a precision of 0.01‰ to 0.025‰ (1SE). Afterwards, the resultant $\Delta_{47(ARF)}$ values are converted to the I-CDES scale for an acid reaction temperature of 90°C to represent the clumped data ($\Delta_{47(ICDES)}$) in a universally consistent reference frame using ETH1, ETH2, ETH3 and ETH4 with the accepted $\Delta_{47(ICDES)}$ values of 0.2052±0.0031‰, 0.2085±0.0030‰, 0.6132±0.0027‰ and 0.4505±0.0035‰, respectively (Bernasconi et al., 2021). $\Delta_{47(ICDES)}$ of studied samples (n=47) varies between 0.27‰ and 0.71‰.

For low-Mg calcites with $\Delta_{47(ARF)}$>0.56‰, precipitation temperatures were estimated using the ARF-based calibration of ref. (Zaarur et al., 2013), for a temperature range of 1–65°C. Remaining low-Mg calcites were corrected using the calibration of ref. (Kluge et al., 2015) for the 25–250°C temperature range, modified with the correction factor of ref. (Banerjee and Ghosh, 2023). The carbonate precipitation temperature was also estimated using the I-CDES scale, based on the proposed calibration equation (Anderson et al., 2021). The low-Mg calcite temperatures agree within uncertainty between ARF and I-CDES calibrations. In this study, I-CDES-based temperature is used for interpretation. The $\delta^{18}O$ of seawater ($\delta^{18}O_{Water}$), from which the carbonates precipitated at thermodynamic equilibrium, was obtained using empirical relationships (Kim and O'Neil, 1997; Müller et al., 2019). Those empirical relationships and temperature calibration equations used in the present study are provided in Table S1. All isotopic analyses were carried out at the Centre for Earth Sciences of the Indian Institute of Science, Bengaluru.

2.3. XRD analysis

To determine the mineralogical components and their relative modal abundances, bulk powdered samples were analysed using Malvern Panalytical's XPERT-PRO Single Crystal XRD equipment in the Department of Geological Sciences at Jadavpur University, Kolkata.

3. Results and Discussion

3.1. Latitudinal Controls on the Carbon Isotopic Composition of Marine Carbonate ($\delta^{13}C_{Carb}$) and Oxygen Availability during Post-Marinoan Carbonate Deposition

Post-Marinoan carbonates, comprising dolostone or limestone interbedded with mudstone, exhibit distinctive marine biochemical signatures marked by negative $\delta^{13}C_{Carb}$ excursions, indicating a shift in the ocean biogeochemical cycle. The magnitude of the isotopic composition varied latitudinally, with equatorial regions registering higher organic productivity and relatively heavier carbonate $\delta^{13}C$ values (Figure 1a). These post-Marinoan carbonates are exposed globally, including in South China, Australia, Namibia, Oman, Siberia, Mongolia, Canada, and India (Hoffman, 2011; Yu et al., 2020). Figure 1b illustrates the distribution of 19 post-Marinoan carbonate exposures from several continents (Excel S1 and https://doi.org/10.5281/zenodo.18507722), including the Badami carbonate, plotted against paleo-latitudinal positions obtained from paleomagnetic reconstructions of continental configurations at ~608 Ma(Cao et al., 2024).

The Badami carbonate deposit comprises two main lithological units (as members) precipitated during the post-glacial marine transgression: the lower Halkurki carbonaceous shale and the upper Konkankoppa limestone. These lithological units are underlain by a lowermost conglomerate and sub-arkosic sandstone-dominated fluvial interval, which grades upward into a marine shale-sandstone assemblage through an intervening sharp ravinement surface (Dey et al., 2009; Mukhopadhyay et al., 2014). The Badami carbonate and shale units exhibit shallow-marine sedimentary structures, including planar lamination, wavy parallel lamination, and hummocky and swaley cross-stratification (Figure S1). Based on similarities in lithofacies and sedimentary structures (Figure S1 and https://doi.org/10.5281/zenodo.17412794), these units resemble the carbonate-bearing litho-units overlying Marinoan cap carbonate units in other chronologically established lithological sections worldwide. This relationship is further substantiated by the radiometric age of the Konkankoppa limestone, dated at 604±25 Ma (George et al., 2023). Carbon isotope stratigraphy of the Badami carbonate deposit displays distinct positive and negative $\delta^{13}C_{Carb}$ excursions, comparable to the carbon isotopic shifts observed in Member 2 of the Ediacaran Doushantuo Formation in South China (Zhou et al., 2019), which directly overlies the Marinoan cap carbonate unit, **referred to as**Doushantuo Member 1 (Figure S2).

A latitudinal variation of the average $\delta^{13}C_{Carb}$ values from carbonate successions equivalent to Member 2 of the Doushantuo formation is documented using carefully selected 19 well-dated, globally distributed post-Marinoan carbonate exposures (Figure 1b, Excel S1). The average $\delta^{13}C_{Carb}$ values for each location are segregated at 30° latitudinal intervals, revealing an overall isotopic enrichment toward lower latitudes (Figure 1a). This pattern resembles modern-day open-ocean settings, such as the mid-Pacific, where the carbon-isotopic composition of dissolved inorganic carbon ($\delta^{13}C_{DIC}$) decreases with increasing latitude (Ge et al., 2022). The $\delta^{13}C_{DIC}$ pattern in the modern-day Pacific Ocean, showing an inverse relationship with the apparent oxygen utilisation (AOU) (Ge et al., 2022). This is translated here into an empirical relationship between $\delta^{13}C_{Carb}$ at equilibrium and AOU (Figure S3.c).

The post-Marinoan Ediacaran carbonates were deposited predominantly in a shallow-marine shelf environment, forming an extensive carbonate platform (Yu et al., 2020). This interval predates the evolution of terrestrial plants, and available constraints suggest that atmospheric oxygen levels had risen to more than ~10% of the present atmospheric level by this time (Casado, 2021). Under such conditions, shallow-marine settings are expected to have been largely oxic to sub-oxic during carbonate precipitation. In the absence of significant terrestrial organic matter input, the Ediacaran marine carbon cycle is best compared to that of the modern open ocean, particularly the mid-Pacific, where terrestrial influence is minimal, providing an appropriate analogue for evaluating the controls on the carbon isotopic composition of dissolved inorganic carbon ($\delta^{13}C_{DIC}$) during the post-Marinoan interval. Accordingly, the modern AOU-$\delta^{13}C_{DIC}$ relationship, observed in the Pacific, can therefore serve as a framework for inferring relative variations in AOU during the post-Marinoan interval. Support for this approach is provided by the latitudinal distribution of $\delta^{13}C_{Carb}$ values in post-Marinoan carbonates (Figure 1), which show enrichment at low latitudes and progressive depletion toward higher latitudes, closely resembling the present-day latitudinal gradient in $\delta^{13}C_{DIC}$ observed in the Pacific Ocean (Ge et al., 2022). Because $\delta^{13}C_{Carb}$ records the carbon isotopic composition of ambient seawater DIC at the time of carbonate precipitation, the observed latitudinal trends in $\delta^{13}C_{Carb}$ values from post-Marinoan shallow-marine carbonates provide a proxy for relative AOU variations during the Ediacaran, grounded in the modern empirical relationship (Excel S1, https://doi.org/10.5281/zenodo.18507722 and Figure S3.c). Figure 1a shows that the estimated AOU anomaly is lower at low latitudes, suggesting reduced aerobic respiration or OM degradation and supporting the idea of burial of organic carbon in the equatorial tropical region. This inference is supported by higher TOC content recorded in the Neoproterozoic postglacial shales from paleo-equatorial tropical regions such as Oman (TOC_{avg}= 3-4wt%) and India (TOC_{avg}= >10wt%) (Xiao et al., 2021), indicating substantial accumulation of OM following the Marinoan glaciation.

3.2. Paleogeographic location and comparison with Ediacaran Doushantuo formation in South China: Chronological framework for Badami sedimentation

The Pb-Pb isochron age assigned to Konkankoppa limestone is 604±25 Ma (George et al., 2023), equivalent to the lower Doushantuo Formation of South China, the Infra Krol Formation of Northern India, the Masirah Bay Formation of Oman, the Brachina Formation of South Australia, the Noonday Formation of California, and the Maieberg Formation of Namibia (Jiang et al., 2007). The Konkankoppa Limestone preserves a primary $^{87}Sr/^{86}Sr$ isotopic ratio of 0.70781, which matches the global Proterozoic marine Sr isotopic value, confirming an additionally suggestive depositional age and primitive nature of the Badami carbonates (George et al., 2019; George et al., 2023). Furthermore, this is comparable to the Sr isotopic composition reported from the lower Doushantuo Formation (Jiang et al., 2007). The Badami carbonate was deposited in a marginal to shallow marine setting (Sen et al., 2025) of the Ediacaran age, and notably lacks an underlying Marinoan cap carbonate litho-unit. According to the paleomagnetic reconstruction of the continental configuration and position

of the Indian Plate during the Ediacaran period, the Badami carbonate sedimentation occurred near the tropical region (Cao et al., 2024; Li et al., 2013). The lack of cap carbonate during Badami sedimentation is probably on account of a “Slush ball” scenario envisaged in the tropics during the post-Marinoan Period (Sen et al., 2025), similar to the cryoconite pond scenario from the Nantuo Formation (Song et al., 2023).

In order to constrain the depositional time interval for the Badami carbonate sedimentation (~20m thick), the $\delta^{13}C_{Carb}$ stratigraphy of the Badami carbonate deposit is compared with that of the Ediacaran Doushantuo Formation from South China, which was also located in the tropics at ~600 Ma (Cao et al., 2024; Li et al., 2013). $\delta^{13}C_{Carb}$ excursions identified in the studied stratigraphic profile (Figure 2a, Figure S2) correlate with the EP1, WANCE and EN2 excursions present in the Doushantuo Formation, anchoring the average depositional age of the Konkankoppa Limestone at ~604 Ma (George et al., 2023; Zhou et al., 2019). The chronological framework, combined with the $\delta^{13}C_{Carb}$ stratigraphic correlation, yields a depositional time interval of ~35 million years (My) for the sedimentation of Badami carbonate, with the lowermost and uppermost boundaries formed at ~626 Ma and ~591 Ma, respectively (Figure S2). Given the absence of sedimentary hiatuses or erosional surfaces within the stratigraphic profile, sedimentation was continuous, providing a unique opportunity for the reconstruction of environmental conditions.

3.3. Depth-bound variability of stable isotopic compositions of the Badami carbonate deposit

A ~20m thick Badami carbonate deposit comprising shale-carbonate intercalation and limestone lithology is investigated for its stable isotopic compositions. These carbonates are primarily composed of micrite, with occasional sparry calcite, as well as the presence of clay minerals and organic matter. The lithology was previously investigated for fossil evidence of Ediacaran affinity (Viswanathiah et al., 1976). The negligible $\delta^{13}C_{Carb}$-$\delta^{18}O_{Carb}$ relationship ($r^2 = 0.00003$), $\delta^{18}O_{Carb}$ values mostly > –10‰ (Knoll et al., 1995), low Mn/Sr (<8) and Fe/Sr (<40) ratios, consistent Pb-Pb age (George et al., 2023) and poor relationship between $\delta^{18}O_{Carb}$ and Mn/Sr ratio are indicative of its primitive composition, qualifying as a reliable proxy for ancient environmental reconstruction (Kaufman and Knoll, 1995; Veizer, 1983). Carbonates from the Halkurki carbonaceous shale recorded an average $\delta^{13}C_{Carb}$ value of 2.31‰, with a range from 1.10‰ to 3.04‰ (Table 1). Similarly, the average $\delta^{13}C_{Carb}$ of Konkankoppa limestone is 0.85‰, with a range from -1.45‰ to 3.77‰ (Table 1), which is lighter than that of Halkurki carbonaceous shale. The cyclicity of the sedimentation process in association with microbial activity and differential degradation of OM is reflected in the carbon isotopic profile from Halkurki to the Konkankoppa member. The positive excursions of $\delta^{13}C_{Carb}$ indicate higher paleo-productivity (Figure 2a): one is registered in the Halkurki carbonaceous shale Member and another in the Konkankoppa limestone Member. Similarly, two negative excursions marked by $\delta^{13}C_{Carb}$ values of -1.39‰ and -1.45‰ are confined in the lower and upper beds of the Konkankoppa limestone Member, respectively (Figure 2a, Table 1). Such fluctuations in $\delta^{13}C_{Carb}$ in the Neoproterozoic sediments are commonly linked to the differential degradation of OM and incorporation of recycled lighter carbon isotope into marine dissolved inorganic carbon (DIC) pool.

Carbon isotopic composition of carbonate-associated OM ($\delta^{13}C_{Org}$) varies between -28.01‰ and -23.24‰ (Figure 2b, Table 1). The relationship between the $\delta^{13}C$ of coexisting carbonate ($\delta^{13}C_{Carb}$) and organic matter ($\delta^{13}C_{Org}$) is examined to detect changes in the ancient pool of DIC using the mass balance approach, where $\delta^{13}C_{Carb}$ and $\delta^{13}C_{Org}$ are expected to covary (Johnston et al., 2012; Oehlert and Swart, 2014). On the other hand, decoupling of $\delta^{13}C_{Carb}$ and $\delta^{13}C_{Org}$ denotes input of CO_2 from the oxidation (degradation) of OM, facilitating the development of organic alkalinity (Hunt et al., 2025). Considering that the atmospheric oxygen level was >10% of the present-day value (Cañadas et al., 2022; Casado, 2021; McFadden et al., 2008; Schrag et al., 2013), the depth of oxygen minima during the Neoproterozoic time interval varied spatially across the marine settings. Near the equator, a slow sedimentation rate in a shallow marine environment (Cantine et al., 2024) may have favoured prolonged organic matter degradation, enhancing alkalinity generation in a manner analogous to processes observed in modern-day large inland seas (Ren et al., 2025). The decoupling behaviour is most prominent at 10m height in the stratigraphic profile, where $\delta^{13}C_{Carb}$is substantially lighter and coincides with a drop in TOC content (Figure 2f), a condition best explained by the degradation of OM. A heavier composition recorded in the $\delta^{13}C_{Org}$ of residual OM is consistent with observations from an incubation experiment on organic molecules, where both oxic and anoxic degradation led to progressive ^{13}C enrichment by 2‰ to 7‰ (Sun et al., 2004). Similar ^{13}C enrichment patterns are observed in the particulate organic carbon and amino acids in the modern-day bottom waters of the Northern South China Sea (Yang et al., 2020). The process of biodegradation continues even in the sedimentary column as exemplified by the variability plot of TOC content and $\delta^{13}C_{Org}$, where higher Mn and lower Fe content are recorded in samples with relatively high TOC content (Figure S4). Given that the Badami carbonates were deposited under oxic to dysoxic conditions (https://doi.org/10.5281/zenodo.17412794), sedimentation rate and temperature would have played a crucial role in controlling the magnitude of OM degradation (Marais et al., 1992). Samples exhibiting low clumped isotope temperatures and high TOC content support in situ OM preservation at lower temperatures.

The oxygen isotopic composition of the carbonate ($\delta^{18}O_{Carb}$) from the Halkurki and Konkankoppa members (Figure 2c) ranges from -10.84‰ to -3.84‰ VPDB, which is comparable with the $\delta^{18}O$ of pristine carbonates precipitated in global oceanic basins at ~600Ma (Isotope Data - mysite.science.uottawa.ca/jveizer/isotope_data/index.html), but remarkably lighter than the modern-day marine carbonate. The $\delta^{18}O_{Carb}$ values align with independent evidence of lighter marine water composition inferred from phosphate-bound oxygen isotopes from the Ediacaran sediments (Fan et al., 2025). The Halkurki Member exhibits an average $\delta^{18}O_{Carb}$ value of -8.21±1.35‰, suggesting relatively less variability in the reservoir water's oxygen isotopic values. From 8m to 12m stratigraphic height, $\delta^{18}O_{Carb}$ values are scattered with a range between -11‰ and -4.61‰, marking the lithological transition from Halkurki to Konkankoppa Member. The heavier composition indicates a dominance of oceanic water during the transition from a marginal to a shallow marine setting (https://doi.org/10.5281/zenodo.17412794). The overlying sediment column is characterised by lighter $\delta^{18}O_{Carb}$ with an average value of -8.15 ± 1.05‰.

3.4. Resetting of carbonate Clumped Isotopic composition in Badami carbonates and estimation of water composition

Carbonate clumped isotopic composition (Δ_{47}) is susceptible to resetting during burial and post-depositional alteration. The important governing factor for such resetting is the time duration of water-rock interaction, which allows the resetting of the carbonate lattice through order-disorder reactions (Ghosh et al., 2006; Passey and Henkes, 2012). Clumped isotope thermometry of the Badami carbonates reveals a wide range of apparent temperatures, spanning 2 ± 2°C to 155 ± 9°C, with more than 90% of the data points falling below 100°C (Table 1). The carbonate deposit investigated here is the uppermost unit of the Badami Group (Dey, 2015) and therefore underwent a limited burial and exhumation process, insufficient to reset the original clumped composition, including disturbance of geochronometers (George et al., 2023). Geochemical evidence for the least alteration and preservation of the pristine character is previously described in section 3.3.

The carbonate mineralogy is dominated by low-Mg calcite, with only three out of nineteen samples, placed in the upper stratigraphic segment, showing the presence of dolomite. These samples exhibit significantly elevated Δ_{47} temperatures (>100°C), interpreted as products of dolomitization in the presence of hydrothermal fluid, supported by an enrichment of ~2‰ in $\delta^{18}O_{Carb}$ relative to the observed average $\delta^{18}O_{Carb}$ values of all the samples in the stratigraphic profile. The low apparent temperature members (2-26°C) are represented by five samples (low Mg-Calcite), marking the lowest temperature within each 4m height interval along the stratigraphic profile, interpreted as pristine (Figure 2d). These samples originate from the region of calcite precipitate dominated by micrite in slab sections (Figure S5). Moderately elevated temperatures indicate partial clumped isotope resetting during burial in a closed system. Overall, the Badami carbonates have largely escaped fluid-buffered (open-system) diagenesis, as indicated by isotopic and elemental data. However, the signature of rock-buffered, closed-system burial was evident, particularly in samples with higher Δ_{47}-based temperature estimates and evidence of sparite precipitation (Figure S6).

The ambient temperature recorded in Badami carbonates is comparable with the estimated sea surface temperature deduced from multiple proxies. Ediacaran sea surface temperature estimated from $\delta^{18}O$ of phosphates in shales and carbonates from Doushantuo formation ranges from ~0°C to 31°C (Fan et al., 2025), justifying the retention of pristine composition. In contrast, dolomites from Member 2 of the Doushantuo Formation yield clumped-isotope temperatures ranging from 55°C to 155°C, attributed to early diagenetic solid-state reordering (Chang et al., 2020). Dolomites from the Ediacaran Khufai Formation in Oman yield clumped-isotope temperatures ranging from 28.8±(5.9, 6.3)°C to 75.1±(15.0, 17.2)°C (Bergmann et al., 2025). Heavier $\delta^{18}O$ signatures in coeval phosphates and dolomites from the Doushantuo Formation are interpreted as pristine, yielding paleotemperatures of 32.2-34.0°C (Ling et al., 2004). Independent estimates from primary fluid inclusions in Sinian-age halite indicate homogenization temperatures ranging from 13.3±1.0°C to 39.4±1.0°C, with a majority clustering around 20-25°C (Meng et al., 2011). Additional reconstructions using $\delta^{18}O_{Carb}$ (~50°C; (Jaffrés et al., 2007)), $\delta^{30}Si$–$\delta^{18}O$ of cherts (25-35°C;(Robert and Chaussidon, 2006)), and COPSE (Carbon, Oxygen, Phosphorus, Sulphur and Evolution) model outputs (15-20°C;(Mills et al., 2019)) collectively support a moderately warm Ediacaran Ocean (~605 Ma). The Δ_{47} temperatures reported in the present study reveal the first evidence of low-temperature carbonate formation in a tropical setting, showing minimal post-depositional alteration, and the well-preserved OM within these carbonates exhibits thermal sensitivity.

The estimated oxygen isotopic composition of seawater ($\delta^{18}O_{Water}$) varies from -11.49‰ to 10.14‰ in the VSMOW scale (Figure 2e). Lighter compositions mark the presence of freshwater, and the heavier compositions either denote evaporation or interaction with mantle-derived hydrothermal water (Banerjee et al., 2023). The $\delta^{18}O_{Water}$ estimated from the low-temperature endmember ranges between -11.49‰ and -4.36‰, indicating freshwater dominance in the depositional environment. In the stratigraphic profile, lighter $\delta^{18}O_{Water}$ coincides with high TOC and $\delta^{13}C_{Carb}$, reflecting freshwater-driven biogenic activity during Badami carbonate deposition (Figure 2a, 2e, 2f).

3.5. Role of temperature on organic matter (OM) degradation, attributed to aerobic conditions for the degradation.

The carbon isotope ratio of organic matter in the Neoproterozoic sediments signifies several processes, including photosynthesis, chemosynthesis, and OM degradation in the absence of terrestrial organic input. The Neoproterozoic carbonate sediments are characterised by multiple negative $\delta^{13}C_{Carb}$ shifts that occurred over tens of millions of years. Such $\delta^{13}C_{Carb}$ patterns are generally used to estimate carbon burial in the ocean and its relationship with environmental oxygen availability. If this $\delta^{13}C_{Carb}$ shift indicates the change in the oceanic dissolved carbon pool, then $\delta^{13}C_{Carb}$ and $\delta^{13}C_{Org}$ are expected to covary (Johnston et al., 2012). However, several Neoproterozoic records indicate a decoupling pattern between $\delta^{13}C_{Carb}$ and $\delta^{13}C_{Org}$, as observed in the present study, suggesting in situ OM degradation generating organic alkalinity (Hunt et al., 2025). To understand the decoupling pattern between $\delta^{13}C_{Carb}$ and $\delta^{13}C_{Org}$, a mathematical model is proposed here to obtain the mechanism of in situ OM degradation, utilising the concept of Rayleigh fractionation. The model presents the $\delta^{13}C_{Org}$ evolution of the residual OM pool during the degradation process, which covaries with ambient temperature. Here, we drew an analogy with the process of biodegradation in the soil environment, where the $\delta^{13}C_{Org}$ of residual OM in the reservoir became progressively heavier with progressive degradation under aerobic conditions (Wynn, 2007). This model explains the relationship between $\delta^{13}C_{Org}$ of a reservoir and the fraction of organic carbon remaining in the reservoir following degradation (f). This relationship is given by the equation;

$$\delta = \delta o f^{\rho} + [1-f^{\rho}]*(\beta\delta_r - \varepsilon)/(\alpha+\beta-1) \quad (1)$$

Here $\delta = \delta^{13}C_{Org}$ of an organic carbon reservoir at any instance of time, δo= initial $\delta^{13}C_{Org}$ of that reservoir, $\delta_r = \delta^{13}C_{Org}$ of organic matter added to the reservoir, β= ratio of organic carbon added to the reservoir to that removed in a steady state condition where, α= fractionation factor of carbon isotope between the organic carbon leaving and left behind the reservoir, ε (enrichment factor) = (α-1) x10^3, ρ= α/(1- β)-1. ε is adopted as -2 (Šantrůčková et al., 2000; Wynn, 2007). This enrichment factor is observed in the incubation experiment during the oxic and anoxic degradation of organic molecules (Sun et al., 2004). For this model, we assume that the reservoir is isotopically well-mixed and the δ_r value is -25‰ (mean $\delta^{13}C_{Org}$ value of the Proterozoic Ocean) (Marais et al., 1992; Schidlowski, 2001). When carbon is added to the reservoir, there is no isotopic fractionation; however, isotopic fractionation occurs during the removal process.

The temperature dependency of OM degradation in the Neoproterozoic Badami carbonate deposit is recorded in this study. The elevated atmospheric oxygen level (Cañadas et al., 2022; Casado, 2021; McFadden et al., 2008; Schrag et al., 2013) led to increased oxygen abundance in the reservoir, thereby promoting OM degradation (Tatzel et al., 2017) and the development of alkalinity (Hunt et al., 2025). Equation (1) is suitable to explain the degradation process, where OM is added to the reservoir by photosynthesis or chemosynthesis and removed from the reservoir by oxidation or decomposition. The lowest $\delta^{13}C_{Org}$ value (-28.01‰) among the studied samples is taken as the initial isotopic composition (δo), assuming it represents the initial state. The remaining fraction of organic carbon (f) for each sample is calculated as the TOC content of the individual sample divided by 0.49 wt%, the highest TOC content measured among all studied samples. Stratigraphically, samples registering the highest TOC content and the lowest $\delta^{13}C_{Org}$ are closely positioned. Figure 3 illustrates the degree of OM decomposition and the impact of ambient temperature. Here, we have utilised carbonate clumped isotope-based temperature estimates (obtained from bulk powdered samples) to elucidate the temperature dependency of OM decomposition. The dolomitic samples displaying very high temperature (>100°C) are placed beyond the β=0 curve. It indicates that these samples are almost devoid of organic carbon (TOC=0.03-0.07wt%) and were formed during hydrothermal fluid interaction; the original OM was entirely removed. Accordingly, the cogenetic inorganic carbonate phase acquired a relatively lighter $\delta^{13}C_{Carb}$ with an average of 1.3‰. Most of the calcites exhibiting moderate to high temperatures (44°C to 100°C) are placed near the β=0 and β=0.2 contour, indicating 80–100% decomposition of the organic carbon associated with the carbonate sediment. Samples following the β=0.5 curve contain a higher amount of remaining organic fraction (1 to 0.8) and are categorised into two distinct types based on temperature ranges: 28°C to 47°C (3 samples) and approximately ~85°C (2 samples). The temperature dependence of OM degradation is consistent with samples exhibiting a temperature range of 28°C to 47°C; a higher f value implies less degradation. However, samples exhibiting high temperatures (~85°C), a large remaining organic fraction, and a lower rate of organic decomposition (β > 0.5) are thought to have formed under conditions of either high sedimentation rate or relative anoxia. The sample, showing a low temperature (14°C), is placed on the β=0.8 curve, implying a loss of 20% original OM during degradation.

3.6. Reconstruction of the Depositional environment based on integrated analysis of stable isotope and Total organic carbon (TOC) content along with sedimentary facies.

To reconstruct the depositional environment of the Badami carbonates, we integrate sedimentary facies analysis with $\delta^{13}C_{Carb}$, TOC content, and $\delta^{13}C_{Org}$ signatures, drawing comparisons with the well-studied litho-sections of the Ediacaran Doushantuo Formation in South China. For this purpose, we have compiled TOC content, $\delta^{13}C_{Carb}$ and $\delta^{13}C_{Org}$ data from shale-carbonate assemblages across multiple sections exposing Member 2 of the Doushantuo Formation, deposited in shelf-to-slope-basin settings (Excel S2), as Member 2 is considered coeval with the Badami carbonate deposit (Section 3.2). Paleogeographic reconstructions place both India and South China in equatorial tropical latitudes ~604Ma (Cao et al., 2024; Li et al., 2008; Li et al., 2013), providing a suitable basis for inter-basin comparison of depositional processes and biogeochemical signatures.

The depositional environment of the Doushantuo Formation is well-constrained by facies analysis and Ediacaran biota distribution, with Member 2 representing a complete litho-unit from transgressive systems tract (TST) to highstand systems tract (HST), deposited across a range of environments from intrashelf lagoons (partially to fully restricted) to open marine (Jiang et al., 2011; Xiao et al., 2021). Geochemical signatures from these environments reveal a systematic gradient in TOC content, $\delta^{13}C_{Org}$ and $\delta^{13}C_{Carb}$ values, with the intrashelf lagoonal setting marked by low TOC content but elevated $\delta^{13}C_{Carb}$ values relative to slope and basinal settings (Figure 4). The low TOC in lagoonal carbonates reflects limited OM preservation, despite high primary productivity. This poor preservation is attributed to shallow, oxygen-rich water columns, which prompted the intensification of aerobic decomposition of OM. Photosynthetic activity in these regions was enhanced by sunlight availability and nutrient supply from catchment runoff and tidal mixing, regulated ^{13}C-enrichment in the dissolved inorganic carbon (DIC) pool, facilitating carbonate precipitation with heavier $\delta^{13}C$ values. In contrast, deeper slope and basin environments were characterised by persistent water column stratification and the development of oxygen minimum zones (OMZs). The resultant euxinic or anoxic bottom water enhanced OM preservation, explaining the relatively high TOC in those settings. Meanwhile, $\delta^{13}C_{DIC}$ values in OMZs were lower due to the OM degradation, while the DIC of surface waters were enriched with ^{13}C. Carbonates precipitated above the OMZs may have positive or near-zero $\delta^{13}C_{Carb}$ values, while carbonate deposits below the OMZs registered significantly negative $\delta^{13}C_{Carb}$ values. Carbonates present in slope setting showed extremely lighter $\delta^{13}C_{Carb}$ values, which were indicative of incorporation of a lighter ^{12}C introduced by the recycling of OM and methane oxidation (Jiang et al., 2011).

There is a significant similarity between the sedimentary facies recognised in the Badami carbonate section and those of the Doushantuo Formation in China. The deposition of the Halkurki carbonaceous shale and the overlying Konkankoppa limestone of the Badami Group occurred during a transgressive phase within a marginal to shallow marine setting, as determined by sedimentary facies analysis (https://doi.org/10.5281/zenodo.17412794). Hence, we extend this approach to the explanation of the coeval Badami carbonates, exhibiting $\delta^{13}C$carb values of up to 3.77‰ and TOC contents of ≤ 0.5 wt%, consistent with deposition in a productive but oxygenated intrashelf-lagoonal setting. The oxidation of OM in the shelf lagoon environment is evident from the observed relative enrichment of $\delta^{13}C_{Org}$ in the studied samples (average $\delta^{13}C_{Org}$= -26.52‰). The occasional water column stratification during transition from a marginal to a shallow marine setting, driven by sea level rise, likely promoted the formation of OMZs, as inferred from two discrete negative excursions in $\delta^{13}C_{Carb}$ stratigraphy (Figure 2a). Sedimentological structures indicative of a shallow marine ecosystem, together with isotopic signatures in carbonates and organic matter, suggest that the Badami carbonates were deposited in a fully to partially restricted, seasonally stratified intra-shelf lagoonal setting.

4. Conclusion

This study examines the paleoenvironmental and geochemical factors influencing organic carbon preservation in the Badami carbonates, providing the first evidence of low-temperature carbonate formation in a tropical setting during the Ediacaran period. The Badami carbonates, deposited in a shallow intra-shelf lagoon, exhibit significant variations in $\delta^{13}C_{Carb}$, $\delta^{13}C_{Org}$, and TOC with a change in ambient temperature. The $\delta^{13}C_{Carb}$ stratigraphy of the Badami carbonate deposit aligns with that of the Doushantuo Formation, indicating coeval deposition from ~626Ma to 591Ma. A decoupling between $\delta^{13}C_{Carb}$ and $\delta^{13}C_{Org}$

reflects enhanced OM degradation in the thermally active sediment-water column. AOU estimates and Rayleigh fractionation highlight seawater temperature as a key player of OM preservation in the environment; cooler intervals favoured preservation, whereas warmer, oxic phases promoted OM degradation. $\delta^{18}O_{Water}$ profiles further suggest freshwater influx and hydrothermal influence during carbonate formation. By comparing the Badami carbonates with Member 2 of the Doushantuo Formation, this study establishes environmental controls on carbon-isotopic trends and on the preservation of organic matter across depositional settings. The intrashelf lagoon environment connected to the open ocean through an epeiric seaway during Badami sedimentation is characterised by higher productivity but low TOC content due to aerobic degradation, as indicated by $\delta^{13}C_{Org}$ enrichment. Collectively, these findings demonstrate how redox conditions, temperature, sedimentation rate, and palaeogeography worked in tandem to shape rapid carbon cycling and OM burial in the Neoproterozoic Ediacaran Ocean.

Declarations

Data source

All stable and clumped isotope data required to evaluate the conclusions in the paper are available at https://doi.org/10.5281/zenodo.18507722. Fe, Mn, and Sr concentration data, as well as XRD data, are available at https://doi.org/10.5281/zenodo.17412794.

Acknowledgments

This work was supported by a research fellowship from the Ministry of Earth Sciences, India, as well as the Divecha Centre for Climate Change, IISc, India, for the Grantham fellowship to RG. We acknowledge the Government of India for granting permission for sampling and for financial support for fieldwork on the Badami carbonates through the DAE-BRNS project (Department of Atomic Energy-Board of Research in Nuclear Sciences; Sanction 966 No. 36(5)/14/03/2018-BRNS with NRFCC, BRNS). We thank Mr Dipayan Biswas and Mr Soumyadeep Bose for helping us collect samples during field work. We thank Ms Shalini Roy for helping with the Kriging software.

References

1. Anderson, N., Kelson, J.R., Kele, S., Daëron, M., Bonifacie, M., Horita, J., Mackey, T.J., John, C.M., Kluge, T., Petschnig, P., 2021. A unified clumped isotope thermometer calibration (0.5–1,100 C) using carbonate-based standardization. Geophysical Research Letters 48, e2020GL092069.
2. Banerjee, S., Ghosh, P., 2023. A correction scheme for calcium carbonate clumped isotope (Δ47) thermometric equation depending on sample preparation technique. Applied Geochemistry 158, 105809.
3. Banerjee, S., Ghosh, P., Banerjee, Y., Riding, R., 2023. Oxygen isotopic composition of Paleoproterozoic seawater revealed by clumped isotope analysis of dolomite, Vempalle Formation, Cuddapah, India. Chemical Geology 621, 121356.
4. Bergmann, K.D., Osburn, M.R., Anderson, N.T., Hayhow, C., Wilcots, J., Cantine, M.D., Fischer, W.W., Bonifacie, M., 2025. Origins and alteration of Ediacaran carbonates recording the Shuram excursion in Oman. Geochemistry, Geophysics, Geosystems 26, e2025GC012161.
5. Bernasconi, S.M., Daëron, M., Bergmann, K.D., Bonifacie, M., Meckler, A.N., Affek, H.P., Anderson, N., Bajnai, D., Barkan, E., Beverly, E., 2021. InterCarb: A community effort to improve interlaboratory standardization of the carbonate clumped isotope thermometer using carbonate standards. Geochemistry, Geophysics, Geosystems 22, e2020GC009588.
6. Bristow, T.F., Kennedy, M.J., Derkowski, A., Droser, M.L., Jiang, G., Creaser, R.A., 2009. Mineralogical constraints on the paleoenvironments of the Ediacaran Doushantuo Formation. Proceedings of the National Academy of Sciences 106, 13190-13195.
7. Cañadas, F., Papineau, D., Leng, M.J., Li, C., 2022. Extensive primary production promoted the recovery of the Ediacaran Shuram excursion. Nature communications 13, 148.
8. Cantine, M.D., Rooney, A.D., Knoll, A.H., Gómez-Pérez, I., al Baloushi, B., Bergmann, K.D., 2024. Chronology of Ediacaran sedimentary and biogeochemical shifts along eastern Gondwanan margins. Communications Earth & Environment 5, 520.
9. Cao, X., Collins, A.S., Pisarevsky, S., Flament, N., Li, S., Hasterok, D., Müller, R.D., 2024. Earth's tectonic and plate boundary evolution over 1.8 billion years. Geoscience Frontiers 15, 101922.
10. Casado, J., 2021. A Review of the Neoproterozoic Global Glaciations and a Biotic Cause of Them. Earth Systems and Environment 5, 811-824.
11. Chang, B., Li, C., Liu, D., Foster, I., Tripati, A., Lloyd, M.K., Maradiaga, I., Luo, G., An, Z., She, Z., 2020. Massive formation of early diagenetic dolomite in the Ediacaran ocean: Constraints on the "dolomite problem". Proceedings of the national academy of sciences 117, 14005-14014.
12. Chen, Z.-y., Zhai, W.-d., Yang, S., Zhang, Y., Liu, P.-f., 2022. Exploring origin of oxygen-consuming organic matter in a newly developed quasi-hypoxic coastal ocean, the Bohai Sea (China): A stable carbon isotope perspective. Science of the Total Environment 837, 155847.
13. Dennis, K.J., Affek, H.P., Passey, B.H., Schrag, D.P., Eiler, J.M., 2011. Defining an absolute reference frame for 'clumped'isotope studies of CO2. Geochimica et Cosmochimica Acta 75, 7117-7131.
14. Dey, S., 2015. Geological history of the Kaladgi–Badami and Bhima basins, south India: sedimentation in a Proterozoic intracratonic setup.
15. Dey, S., Rai, A., Chaki, A., 2009. Palaeoweathering, composition and tectonics of provenance of the Proterozoic intracratonic Kaladgi–Badami basin, Karnataka, southern India: evidence from sandstone petrography and geochemistry. Journal of Asian Earth Sciences 34, 703-715.
16. Fan, H., Chen, Z., Zhang, F., Zhu, C., Du, S., Zhang, Y., Wen, H., Khan, D., Algeo, T.J., 2025. Seawater temperatures during the early to middle Ediacaran: Phosphate oxygen isotope records. Chemical Geology 678, 122642.

17. Fosu, B.R., Ghosh, P., Mishra, D., Banerjee, Y., Sarkar, A., 2019. Acid digestion of carbonates using break seal method for clumped isotope analysis. Rapid Communications in Mass Spectrometry 33, 203-214.
18. Ge, T., Luo, C., Ren, P., Zhang, H., Fan, D., Chen, H., Chen, Z., Zhang, J., Wang, X., 2022. Stable carbon isotopes of dissolved inorganic carbon in the Western North Pacific Ocean: Proxy for water mixing and dynamics. Frontiers in marine Science 9, 998437.
19. George, B.G., Ray, J.S., Kumar, S., 2019. Geochemistry of carbonate formations of the Chhattisgarh Supergroup, central India: implications for Mesoproterozoic global events. Canadian Journal of Earth Sciences 56, 335-346.
20. George, B.G., Ray, J.S., Pillai, S.P., Mahala, M.K., Kumar, S., Kale, V.S., 2023. C-Sr-Pb isotope systematics of the carbonate sequences of Kaladgi Supergroup, India: Implications for basin evolution and correlation with Proterozoic global events. Precambrian Research 388, 107014.
21. Ghosh, P., Adkins, J., Affek, H., Balta, B., Guo, W., Schauble, E.A., Schrag, D., Eiler, J.M., 2006. 13C–18O bonds in carbonate minerals: A new kind of paleothermometer. Geochimica et Cosmochimica Acta 70, 1439-1456.
22. Hazen, R.M., Sverjensky, D.A., Azzolini, D., Bish, D.L., Elmore, S.C., Hinnov, L., Milliken, R.E., 2013. Clay mineral evolution. American Mineralogist 98, 2007-2029.
23. Hoffman, P.F., 2011. Strange bedfellows: glacial diamictite and cap carbonate from the Marinoan (635 Ma) glaciation in Namibia. Sedimentology 58, 57-119.
24. Hunt, C.W., Salisbury, J.E., Liu, X., Byrne, R.H., 2025. Organic alkalinity distributions, characteristics, and application to carbonate system calculations in estuarine and coastal systems. Limnology and Oceanography 70, 319-333.
25. Jaffrés, J.B., Shields, G.A., Wallmann, K., 2007. The oxygen isotope evolution of seawater: A critical review of a long-standing controversy and an improved geological water cycle model for the past 3.4 billion years. Earth-Science Reviews 83, 83-122.
26. Jiang, G., Kaufman, A.J., Christie-Blick, N., Zhang, S., Wu, H., 2007. Carbon isotope variability across the Ediacaran Yangtze platform in South China: Implications for a large surface-to-deep ocean δ13C gradient. Earth and Planetary Science Letters 261, 303-320.
27. Jiang, G., Shi, X., Zhang, S., Wang, Y., Xiao, S., 2011. Stratigraphy and paleogeography of the Ediacaran Doushantuo Formation (ca. 635–551 Ma) in south China. Gondwana Research 19, 831-849.
28. Johnston, D.T., Macdonald, F.A., Gill, B., Hoffman, P., Schrag, D.P., 2012. Uncovering the Neoproterozoic carbon cycle. Nature 483, 320-323.
29. Kaufman, A.J., Knoll, A.H., 1995. Neoproterozoic variations in the C-isotopic composition of seawater: stratigraphic and biogeochemical implications. Precambrian research 73, 27-49.
30. Kaushal, R., Ghosh, P., 2018. Stable oxygen and carbon isotopic composition of rice (Oryza sativa L.) grains as recorder of relative humidity. Journal of Geophysical Research: Biogeosciences 123, 423-439.
31. Kim, S.-T., O'Neil, J.R., 1997. Equilibrium and nonequilibrium oxygen isotope effects in synthetic carbonates. Geochimica et cosmochimica acta 61, 3461-3475.
32. Kluge, T., John, C.M., Jourdan, A.-L., Davis, S., Crawshaw, J., 2015. Laboratory calibration of the calcium carbonate clumped isotope thermometer in the 25–250 C temperature range. Geochimica et Cosmochimica Acta 157, 213-227.
33. Knoll, A.H., Kaufman, A.J., Semikhatov, M.A., 1995. The carbon-isotopic composition of Proterozoic carbonates; Riphean successions from northwestern Siberia (Anabar Massif, Turukhansk Uplift). American Journal of Science 295, 823-850.
34. Laakso, T.A., Schrag, D.P., 2019. A small marine biosphere in the Proterozoic. Geobiology 17, 161-171.
35. Li, Z.-X., Bogdanova, S., Collins, A., Davidson, A., De Waele, B., Ernst, R., Fitzsimons, I., Fuck, R., Gladkochub, D., Jacobs, J., 2008. Assembly, configuration, and break-up history of Rodinia: a synthesis. Precambrian research 160, 179-210.
36. Li, Z.-X., Evans, D.A., Halverson, G.P., 2013. Neoproterozoic glaciations in a revised global palaeogeography from the breakup of Rodinia to the assembly of Gondwanaland. Sedimentary Geology 294, 219-232.
37. Ling, H., Jiang, S., Feng, H., Chen, Y., Chen, J., Yang, J., 2004. Oxygen isotope geochemistry of phosphorite and dolomite and palaeo-ocean temperature estimation: A case study from the Neoproterozoic Doushantuo Formation, Guizhou Province, South China. Progress in Natural Science 14, 77-84.
38. Marais, D.J.D., Strauss, H., Summons, R.E., Hayes, J., 1992. Carbon isotope evidence for the stepwise oxidation of the Proterozoic environment. Nature 359, 605-609.
39. McFadden, K.A., Huang, J., Chu, X., Jiang, G., Kaufman, A.J., Zhou, C., Yuan, X., Xiao, S., 2008. Pulsed oxidation and biological evolution in the Ediacaran Doushantuo Formation. Proceedings of the National Academy of Sciences 105, 3197-3202.
40. Meng, F., Ni, P., Schiffbauer, J.D., Yuan, X., Zhou, C., Wang, Y., Xia, M., 2011. Ediacaran seawater temperature: Evidence from inclusions of Sinian halite. Precambrian Research 184, 63-69.
41. Mills, B.J., Krause, A.J., Scotese, C.R., Hill, D.J., Shields, G.A., Lenton, T.M., 2019. Modelling the long-term carbon cycle, atmospheric CO2, and Earth surface temperature from late Neoproterozoic to present day. Gondwana Research 67, 172-186.
42. Mukhopadhyay, S., Choudhuri, A., Samanta, P., Sarkar, S., Bose, P.K., 2014. Were the hydraulic parameters of Precambrian rivers different? Journal of Asian Earth Sciences 91, 289-297.
43. Müller, I.A., Rodriguez-Blanco, J.D., Storck, J.-C., do Nascimento, G.S., Bontognali, T.R., Vasconcelos, C., Benning, L.G., Bernasconi, S.M., 2019. Calibration of the oxygen and clumped isotope thermometers for (proto-) dolomite based on synthetic and natural carbonates. Chemical Geology 525, 1-17.
44. Oehlert, A.M., Swart, P.K., 2014. Interpreting carbonate and organic carbon isotope covariance in the sedimentary record. Nature Communications 5, 4672.
45. Passey, B.H., Henkes, G.A., 2012. Carbonate clumped isotope bond reordering and geospeedometry. Earth and Planetary Science Letters 351, 223-236.

46. Ramme, L., Ilyina, T., Marotzke, J., 2024. Moderate greenhouse climate and rapid carbonate formation after Marinoan snowball Earth. Nature Communications 15, 3571.
47. Ren, J.-H., Zhu, M.-X., Wang, D.-Y., Li, Q.-Q., Li, T., 2025. Pathways of organic carbon mineralization and benthic fluxes of alkalinity and dissolved inorganic carbon in sediments of large inland seas: The Bohai Sea and North Yellow Sea. Journal of Marine Systems, 104082.
48. Robert, F., Chaussidon, M., 2006. A palaeotemperature curve for the Precambrian oceans based on silicon isotopes in cherts. Nature 443, 969-972.
49. Rukshana, F., 2012. Role of organic matter in soil pH change. La Trobe.
50. Šantrůčková, H., Bird, M., Lloyd, J., 2000. Microbial processes and carbon-isotope fractionation in tropical and temperate grassland soils. Functional Ecology 14, 108-114.
51. Schidlowski, M., 2001. Carbon isotopes as biogeochemical recorders of life over 3.8 Ga of Earth history: evolution of a concept. Precambrian Research 106, 117-134.
52. Schrag, D.P., Higgins, J.A., Macdonald, F.A., Johnston, D.T., 2013. Authigenic carbonate and the history of the global carbon cycle. science 339, 540-543.
53. Sen, A., Mukhopadhyay, S., Stüeken, E.E., Samanta, P., Sarkar, S., Bose, S., Agarwal, S., Kumar, A., 2025. Evolving marine sedimentation, redox stratification, and biogeochemical cycling in mid-to low-latitudinal non-frozen waters during late Neoproterozoic global-scale climatic transitions. Precambrian Research 417, 107661.
54. Sepeda, L., Nogueira, A., dos Santos, R., Okubo, J., Silva, P., Marques, J., Milhomem, J., Luvizotto, G., Macambira, M., Sial, A., 2024. Diagenetic and hydrothermal events revealed by an Ediacaran dolomite breccia from the Araras-Alto Paraguai basin, southern Amazon Craton. Marine and Petroleum Geology 170, 107089.
55. Song, H., An, Z., Ye, Q., Stüeken, E.E., Li, J., Hu, J., Algeo, T.J., Tian, L., Chu, D., Song, H., 2023. Mid-latitudinal habitable environment for marine eukaryotes during the waning stage of the Marinoan snowball glaciation. Nature Communications 14, 1564.
56. Sun, M.-Y., Zou, L., Dai, J., Ding, H., Culp, R.A., Scranton, M.I., 2004. Molecular carbon isotopic fractionation of algal lipids during decomposition in natural oxic and anoxic seawaters. Organic Geochemistry 35, 895-908.
57. Tatzel, M., von Blanckenburg, F., Oelze, M., Bouchez, J., Hippler, D., 2017. Late Neoproterozoic seawater oxygenation by siliceous sponges. Nature Communications 8, 621.
58. Thomas, T.B., Catling, D.C., 2024. Three-stage formation of cap carbonates after Marinoan snowball glaciation consistent with depositional timescales and geochemistry. Nature Communications 15, 7055.
59. Tosca, N.J., Johnston, D.T., Mushegian, A., Rothman, D.H., Summons, R.E., Knoll, A.H., 2010. Clay mineralogy, organic carbon burial, and redox evolution in Proterozoic oceans. Geochimica et Cosmochimica Acta 74, 1579-1592.
60. Van Ryckel, H., Van Aelst, L., van Dael, T., Smolders, E., 2025. Organic matter-mediated leaching of alkalinity in limed acid soils is affected by dissolved organic carbon adsorption and soil structure. EGUsphere 2025, 1-20.
61. Veizer, J., 1983. Chemical diagenesis of carbonates: theory and application of trace element technique.
62. Viswanathiah, M., Venkatachalapathy, V., Khadeer, A., 1976. Microfossils from the Badami Group, Karnataka South India. Journal Geological Society of India 17, 340-345.
63. Wynn, J.G., 2007. Carbon isotope fractionation during decomposition of organic matter in soils and paleosols: Implications for paleoecological interpretations of paleosols. Palaeogeography, Palaeoclimatology, Palaeoecology 251, 437-448.
64. Xiao, D., Cao, J., Luo, B., Tan, X., Xiao, W., He, Y., Li, K., 2021. Neoproterozoic postglacial paleoenvironment and hydrocarbon potential: A review and new insights from the Doushantuo Formation Sichuan Basin, China. Earth-Science Reviews 212, 103453.
65. Yang, Z., Zhang, H., Kang, P., Zhao, Y., Tang, T., 2020. Influence of algal production and decomposition on the carbon isotope signature of labile particulate organic matter on a productive continental shelf under the stress of coastal hypoxia. Frontiers in Marine Science 7, 675.
66. Ye, Z., Zou, N., Zhang, D., Chen, Y., Yin, Y., Feng, X., Du, W., 2025. Sedimentary Environment and Organic Matter Enrichment of Lower Cambrian Niutitang Shales in Fenggang Area, Northern Guizhou: A Case Study of Well YF1. ACS omega.
67. Yu, W., Algeo, T.J., Zhou, Q., Du, Y., Wang, P., 2020. Cryogenian cap carbonate models: a review and critical assessment. Palaeogeography, Palaeoclimatology, Palaeoecology 552, 109727.
68. Zaarur, S., Affek, H.P., Brandon, M.T., 2013. A revised calibration of the clumped isotope thermometer. Earth and Planetary Science Letters 382, 47-57.
69. Zhou, C., Yuan, X., Xiao, S., Chen, Z., Hua, H., 2019. Ediacaran integrative stratigraphy and timescale of China. Science China Earth Sciences 62, 7-24.

Tables

Table 1. Isotopic compositions ($\delta^{13}C_{Carb}$, $\delta^{18}O_{Carb}$, and Δ_{47} in ‰), clumped isotope-based temperature (°C), oxygen isotopic composition of water ($\delta^{18}O_{Water}$ in ‰), carbon isotopic composition of associated organic matter ($\delta^{13}C_{Org}$ in ‰), and TOC content reported from the carbonates of the Badami group.

					ARF Scale				I-CDES Scale (Anderson et al., 2021)				
Sample Name	Height (m)	$\delta^{13}C_{Carb}$ (VPDB) (‰)	$\delta^{18}O_{Carb}$ (VPDB) (‰)	No.	Δ_{47} (‰)	SE Δ_{47} (‰)	Δ_{47} - T (°C)	SE Δ_{47} - T (°C)	Δ_{47} (‰)	SE Δ_{47} (‰)	Δ47-T (°C)	SE Δ_{47}-T (°C)	$\delta^{18}O_{Water}$ (‰)
Point Drill Sample													
HLK1A	0.6	1.85	-3.84	10	0.78	0.01	9	3	0.65	0.01	14	3	-3.77
HLK2B	2.2	2.00	-8.20	9	0.56	0.02	64*	5	0.46	0.02	64	5	1.14
HLK2C	2.2	2.02	-7.03	6	0.58	0.02	60	5	0.48	0.02	58	5	1.33
HLK3	3.9	3.04	-8.80	7	-	-	-	-	-	-	-	-	-
HLK3A	3.9	1.89	-8.60	8	0.65	0.02	37	5	0.54	0.02	39	5	-3.56
HLK4	5.3	2.67	-8.91	7	0.46	0.02	100*	9	0.38	0.02	94	8	4.87
HLK5A	6.7	2.19	-7.90	4	0.72	0.01	20	3	0.61	0.01	24	3	-5.77
HLK5A (Repeat)	6.7	2.18	-7.91	4	0.50	0.01	85*	4	0.41	0.01	82	4	4.12
HLK5B	6.7	2.87	-9.14	11	0.53	0.02	72*	6	0.44	0.02	71	6	1.31
HLK5B (Repeat_1)	6.7	2.94	-7.19	10	0.80	0.01	5	2	0.67	0.01	10	2	-7.92
HLK5B (Repeat_2)	6.7	2.78	-7.48	10	0.81	0.01	2	2	0.68	0.01	8	2	-8.77
HLK5C	6.7	1.93	-8.89	10	0.52	0.02	75*	6	0.43	0.02	74	6	1.97
KNK1A	8.5	-0.76	-8.28	10	0.50	0.01	86*	4	0.41	0.01	82	4	3.85
KNK4	10.1	1.97	-4.61	9	-	-	-	-	-	-	-	-	-
KNK5B	11.5	3.55	-7.47	10	0.57	0.02	62	5	0.48	0.02	59	5	1.10
KNK5A	11.7	3.71	-7.83	8	0.56	0.02	64*	5	0.46	0.02	64	5	1.51
KNK6B	15.1	2.40	-6.98	8	0.69	0.03	29	7	0.57	0.03	32	7	-3.29
KNK6B (Repeat)	15.1	2.48	-9.21	5	-	-	-	-	-	-	-	-	-
KNK6A	15.1	3.77	-8.03	10	0.57	0.02	61		0.48	0.02	59	5	

								5				0.50
KNK6A (Repeat_1)	15.1	3.50	-7.03	10	0.71	0.02	23	4	0.59	0.02	26	4 -4.36
KNK6A (Repeat_2)	15.1	3.64	-8.01	10	0.55	0.01	66*	4	0.45	0.01	66	4 1.65
KNK2'C	18.0	-1.36	-8.81	7	0.52	0.02	77*	8	0.43	0.02	75	7 2.26
KNK2'A	18.0	-0.93	-8.28	10	0.50	0.02	84*	8	0.41	0.02	81	7 3.64
KNK2'A (Repeat)	18	-1.11	-8.24	9	-	-	-	-	-	-	-	- -
KNK2'B	18	-1.24	-8.78	8	0.53	0.02	72*	9	0.44	0.02	71	8 1.64
KNK2'B (Repeat)	18	-0.54	-8.61	8	0.81	0.02	2	3	0.68	0.02	8	3 -9.82
KNK2A	18.2	-1.07	-8.71	8	-	-	-	-	-	-	-	- -
Bulk Powdered Sample												
HLK1	0.6	1.10	-8.97	9	0.65	0.01	40	3	0.56	0.01	34	3 -4.77
HLK2	2.2	2.21	-8.86	7	0.61	0.03	50	7	0.53	0.03	44	7 -2.91
HLK3	3.9	2.43	-9.42	9	0.67	.01	34	4	0.58	0.01	29	3 -6.28
HLK4	5.3	2.63	-9.11	10	0.47	0.01	99*	5	0.39	0.01	92	4 4.30
HLK5	6.7	2.54	-9.38	10	0.47	0.01	97*	5	0.39	0.01	90	5 3.75
KNK1	8.5	-0.91	-10.00	10	0.48	0.02	94*	7	0.40	0.02	87	7 2.74
KNK3A	8.8	-0.40	-8.95	7	0.57	0.02	64	6	0.44	0.01	70	5 1.34
KNK3A (Repeat)	8.8	-0.34	-8.72	10	0.54	0.01	69*	5	0.42	0.01	77	5 2.69
KNK3B	9.1	0.50	-4.94	10	0.65	0.01	38	4	0.51	0.01	48	4 1.71
KNK3B (Repeat)	9.1	0.53	-4.74	10	0.64	0.02	41	5	0.51	0.02	50	5 2.30
KNK4	10.1	1.35	-5.54	10	0.74	0.01	17	2	0.65	0.01	14	2 -5.45
KNK5C	10.3	-1.39	-9.35	10	0.52	0.02	76*	6	0.41	0.02	83	7 2.89
KNK5C (Repeat)	10.3	-1.33	-9.22	10	0.48	0.01	93*		0.37	0.01	97	5

							5					4.94
KNK5B	11.5	3.43	-8.52	10	0.48	0.02	94*	8	0.40	0.02	87	7	4.26
KNK5A	11.7	3.46	-10.84	7	0.60	0.01	54	4	0.51	0.01	47	4	-4.30
KNK6'	13.3	3.50	-8.41	10	0.51	0.01	82*	6	0.39	0.01	88	6	4.56
KNK6	15.1	3.44	-8.56	10	0.50	0.01	86*	4	0.42	0.01	80	3	3.15
SLKL4#	16.6	1.26	-6.76	10	0.41	0.01	-	12	0.32	0.01	125	7	7.20
SLKL3A#	17.3	1.33	-6.48	10	0.38	0.01	-	15	0.29	0.01	143	8	9.03
SLKL3A (Repeat)#	17.3	1.31	-6.38	10	0.35	0.01	-	18	0.27	0.01	155	9	10.14
SLKL3B#	17.3	1.32	-6.53	10	0.41	0.02	-	14	0.32	0.02	124	9	7.35
KNK2'	18.0	-1.45	-8.82	10	0.80	0.01	4	2	0.71	0.01	2	2	-11.49
KNK2' (Repeat_1)	18	-1.25	-9.36	10	0.52	0.02	77*	6	0.40	0.02	84	6	3.02
KNK2' (Repeat_2)	18	-1.18	-9.60	10	0.53	0.02	73*	6	0.41	0.02	81	6	2.28
KNK2	18.2	-1.37	-9.63	10	0.55	0.01	66*	3	0.47	0.01	61	3	-0.74

Dolomitic carbonate samples. Remaining samples are calcite, and for those samples, ARF-based temperature is calculated using the calibration equation provided by Zaarur et al., 2013 (ARF25)(Zaarur et al., 2013) and *Kluge et al., 2015 (CDES90)(Kluge et al., 2015) with a correction factor from Banerjee and Ghosh, 2023(Banerjee and Ghosh, 2023). $\Delta_{47(\text{I-CDES})}$ temperature is calculated using the calibration equation from Anderson et al., 2021 (ICDES90)(Anderson et al., 2021) with a correction factor from Banerjee and Ghosh, 2023(Banerjee and Ghosh, 2023). The water isotopic composition ($\delta^{18}O_{Water}$) is estimated from the I-CDES temperature. $\delta^{18}O_{Water}$ is evaluated using the oxygen isotope fractionation equation proposed by Kim and O'Neil 1997 (Kim and O'Neil, 1997) and Müller et al., 2019 (Müller et al., 2019) for calcitic and dolomitic samples, respectively.

Figures

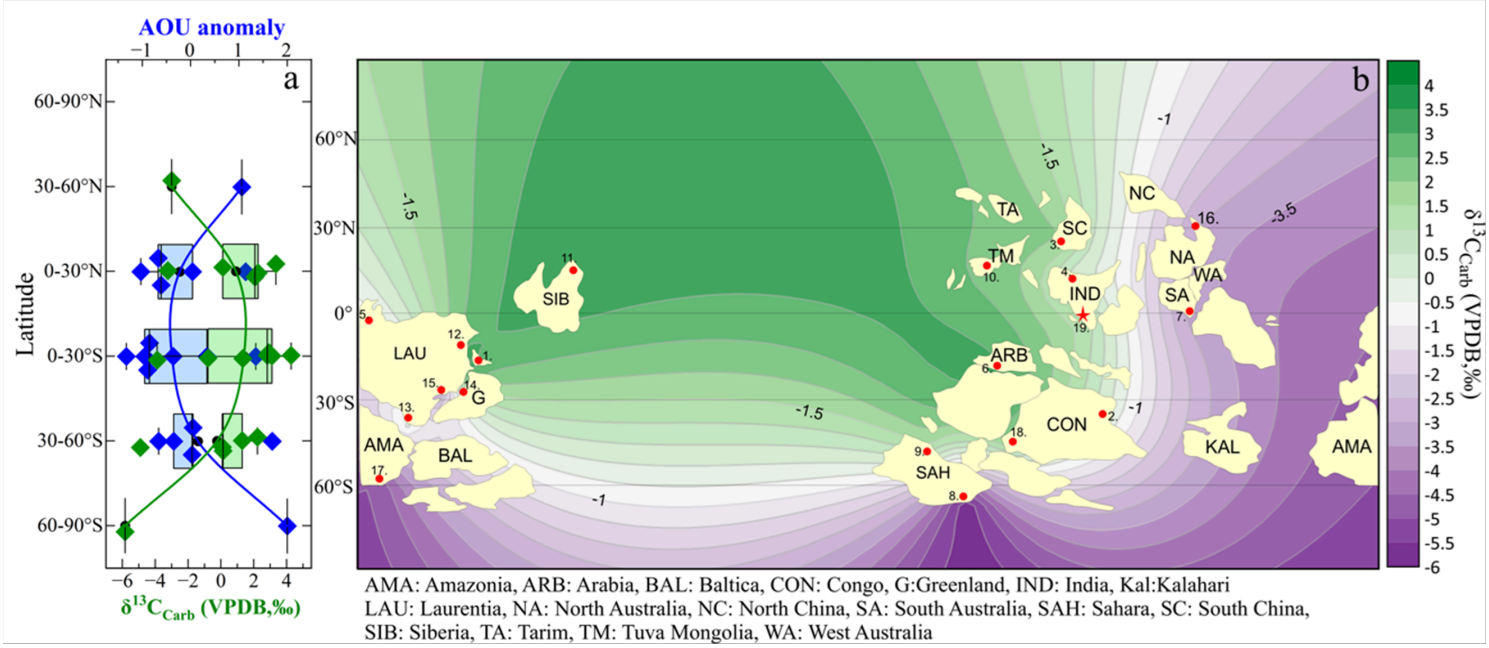


Figure 1

(a) Box plots show the variability in d^{13}C of post-Marinoan carbonates (green) and estimated apparent oxygen utilisation (AOU, blue) across the paleo-latitudes. Each box contains data points of 30° latitudinal intervals. Box brackets delineate 25 and 75 percentiles, while the bar inside the box represents the median of the values. Whiskers indicate 2.5 and 97.5 percentiles. (b) Global distribution of post-Marinoan carbonate deposits (red circles) at ~608 Ma. The Badami carbonate deposit is highlighted as a red star. The Paleo-configuration of continents is adopted from (Cao et al., 2024). The average $\delta^{13}C_{Carb}$ of each carbonate deposit is taken, and the kriging tool is used for the interpolation of intermediate points to understand the latitudinal variation of $\delta^{13}C_{Carb}$ of the post-Marinoan carbonate. Particulars of the numbered red circles are provided in Excel S1 (AOU calculation sheet) and https://doi.org/10.5281/zenodo.18507722.

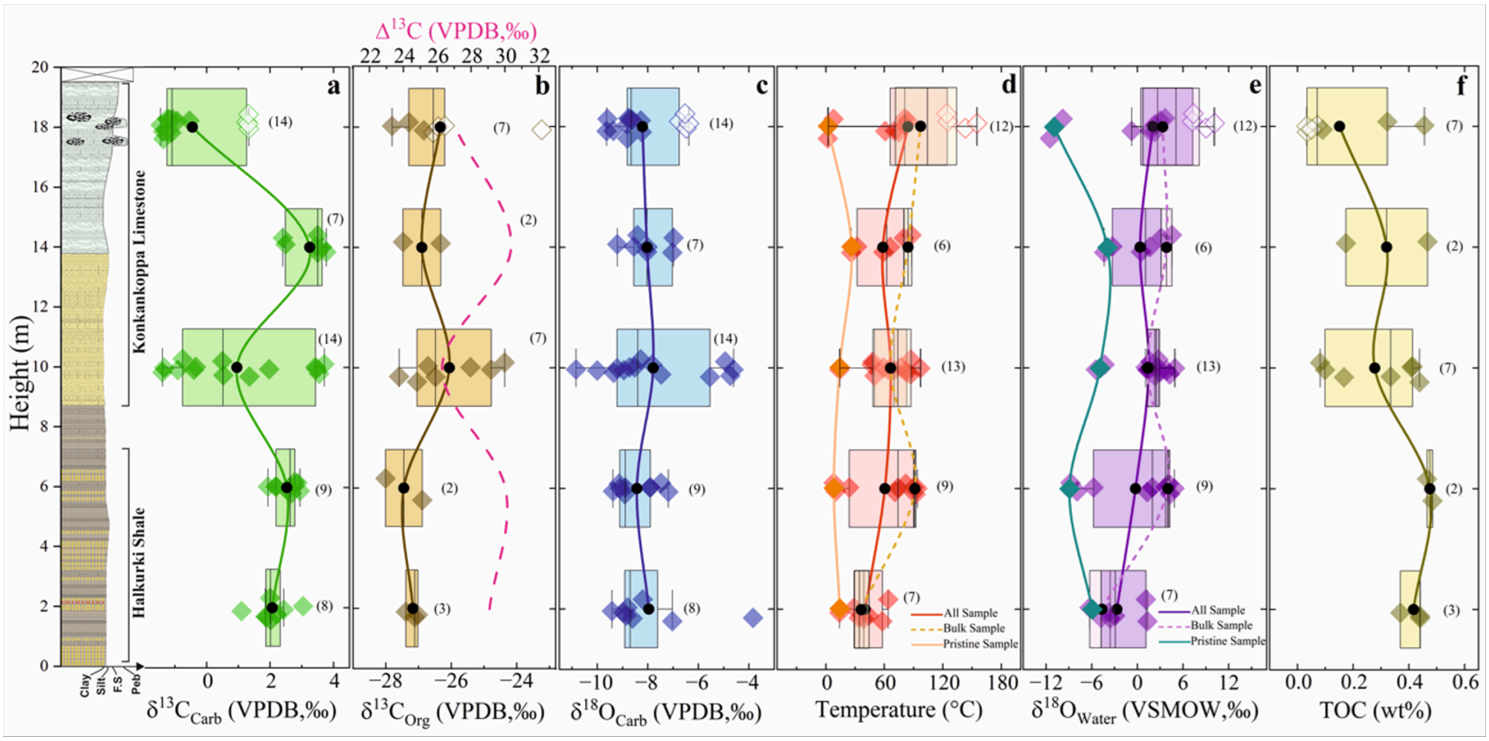


Figure 2

Box plots show the temporal variation in stable isotopic signatures, clumped–isotope–based temperatures, and TOC content from the Badami carbonates and associated organic matter. (a) δ¹³C of carbonate ($\delta^{13}C_{Carb}$, VPDB), (b) δ¹³C of organic matter ($\delta^{13}C_{Org}$, VPDB), $D^{13}C = \delta^{13}C_{Carb} - \delta^{13}C_{Org}$, (c) δ¹⁸O of carbonate ($\delta^{18}O_{Carb}$, VPDB), (d) Carbonate-Clumped-isotope-based temperature (°C), (e) estimated δ¹⁸O of seawater ($\delta^{18}O_{Water}$, VSMOW), and (f) total organic

carbon content (TOC, wt%). Boxes indicate sample groupings along the stratigraphic profile for each 4m height. Box brackets delineate 25 and 75 percentiles, while the bar in the middle of the box represents the median of the values. Whiskers indicate 2.5 and 97.5 percentiles. Calcite and Dolomite samples are represented by filled diamonds and open diamonds, respectively. Symbols of sedimentary structures shown in the stratigraphic profile are described in Figure S1.

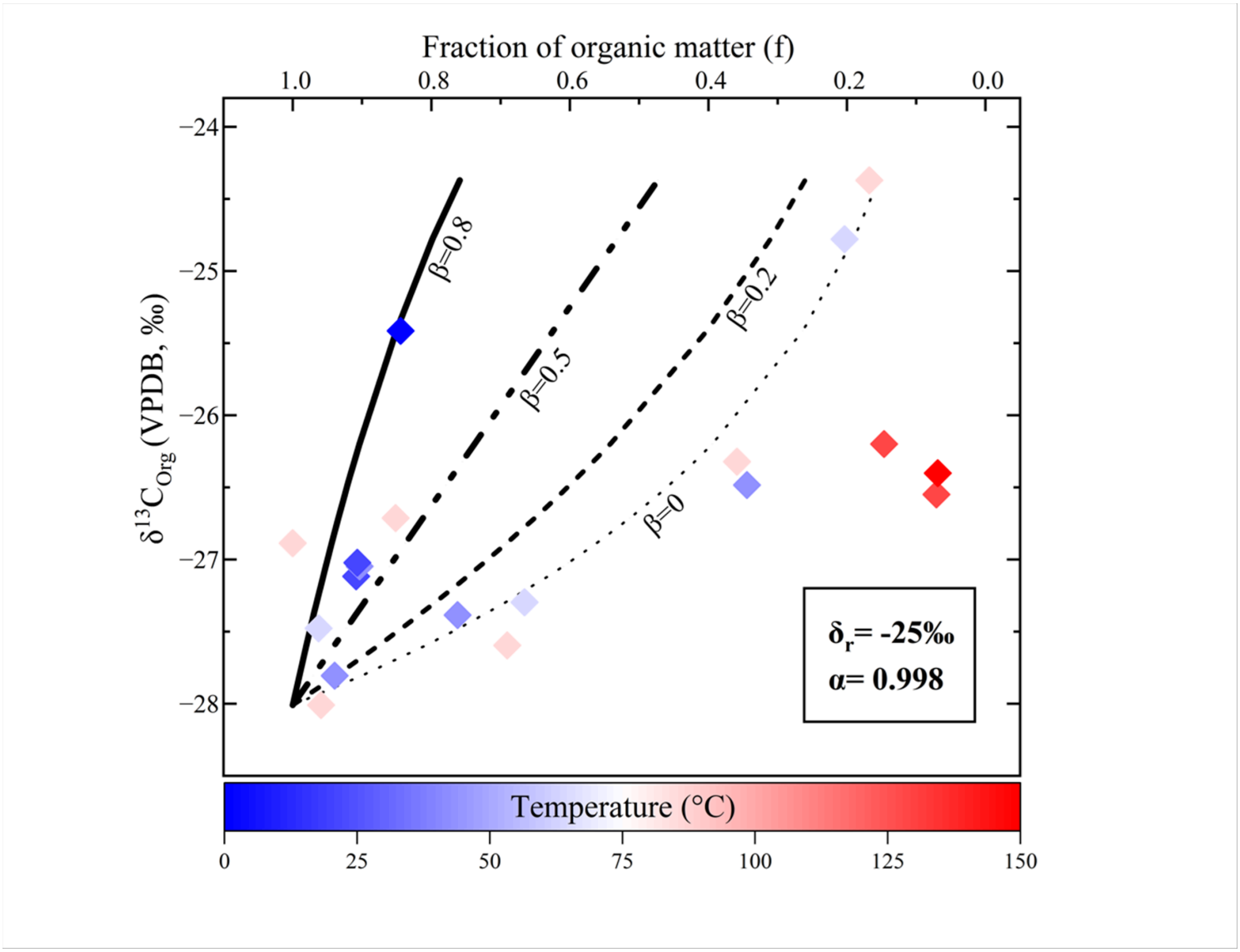


Figure 3

The temperature dependency of organic matter degradation during the sedimentation of Neoproterozoic Badami carbonate, with higher temperatures corresponding to lower TOC contents (remaining organic fraction f) and vice versa. This model is based on the Rayleigh fractionation concept, in which the β factor is defined as the ratio of organic carbon added to the reservoir to that lost by degradation in a steady-state condition. d_r is the carbon isotopic composition of the organic matter added to the reservoir without isotopic fractionation, and a is the fractionation factor between the carbon species leaving the system due to oxidation and the residual organic carbon.

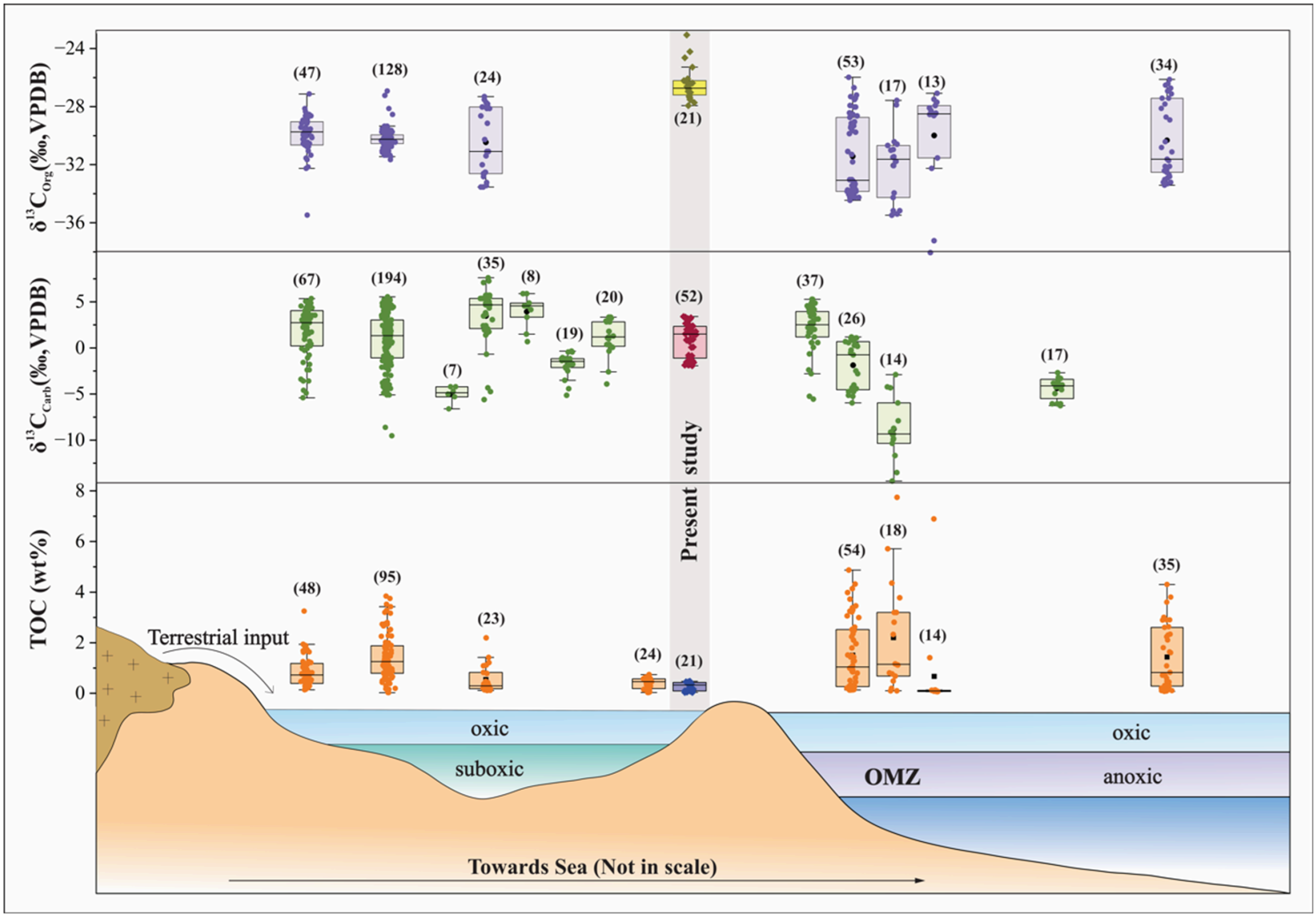


Figure 4

Reconstruction of depositional environment of Badami carbonate deposit using the carbon isotopic composition of carbonates, associated organic matter, and TOC content, drawing a comparison with the geochemical signatures from multiple litho-sections of Member 2 of Ediacaran Doushantuo formation with well-constrained paleogeographic settings. $\delta^{18}O_{Carb}$, $\delta^{18}O_{Org}$ and TOC data from litho-sections of Member 2 of the Doushantuo formation are provided with references in Excel S2 and https://doi.org/10.5281/zenodo.18507722.

Supplementary Files

This is a list of supplementary files associated with this preprint. Click to download.

- Ghoshetal.SupportingInformation.docx